MET O 19 BRANCH MEMORANDUM No. 45.....

Analysis of the balloon Flight of 17 March 1976 which measured atmospheric transmission using a pressure modulator equivalent to the high pressure channel of the Meteorological Office Stratospheric Sounding Unit.

by

D R Pick and B R Barwell Met O 19

July 1978

Met O 19
(High Atmosphere Branch)
Meteorological Office
London Road
BRACKNELL
Berks RG12 2SZ

Analysis of the balloon Flight of 17 March 1976 which measured atmospheric transmission using a pressure modulator equivalent to the high pressure channel of the Meteorological Office Stratospheric Sounding Unit.

D R Pick and B R Barwell Met O 19

July 1978

Abstract

This report describes the preparation, flight and analysis of a successful flight of a pressure modulation cell similar in design to the high pressure channel of the Met. Office stratospheric sounding unit. The measured transmission of sunlight is compared with both pre and post flight laboratory measurements and with theoretical calculation. Within the limitation of the accuracy of the pressure transducer flown, and the uncertainty of the signal scaling and gain constancy, the theoretical calculations agree with the measurement. These uncertainties amount to a transmission error of about 0.02 compared to a required accuracy of $\sim .003$ in τ .

1. Introduction

In order to interpret the output of a satellite radiometer, particularly those measuring above the radiosonde ceiling of $\sim$ 30 km, atmospheric weighting functions need to be calculated. For consistency with instrument noise, the atmospheric transmission height variation (its height derivative is the required weighting function) should be known to about .003. It is difficult to make such calculations to this accuracy due to uncertainty in the details of the line spectra, accuracy of the line width model, the extrapolation of line strength and widths over the atmospheric range of temperature and pressure, and also the uncertainty in the spectral response of the radiometer.

Measurements, of the transmission through various gas paths, made with the radiometer can be used to verify the calculations for a constant length path at uniform pressure and temperature. A better technique is to make transmission measurements on a long path within the free atmosphere.

The Oxford University atmospheric group pioneered the measurement of weighting functions using a White cell for their selective chopper radiometers and the pressure modulation radiometer flown on the Nimbus experimental satellites. In conjunction with NOAA (National Oceanic and Atmospheric Administration) the Oxford group has participated in a balloon programme to make atmospheric transmission measurements in the 15 micron ν_2 band of carbon dioxide. The last two balloon flights (on 3 Dec 1974 and 17 March 1976) incorporated a pressure modulator with similar optical properties to the high-pressure channel (weighting function centred at 15 mb) of the Meteorological Office stratospheric sounding unit for Tiros N.

The technique and results from the earlier flights have been described in detail in the D.Phil theses of J H Batey (1975) and J Delderfield (1977). Several difficulties arose with the December 1974 flight, causing problems with the interpretation of the Oxford results. These were mainly due to a noisy clock, continuous rotation of the balloon (so that the signal levels were periodically interrupted by cables crossing the viewing path), and a noisy window channel. Since NOAA wanted to refly the gondola experiments with a new polarimeter the opportunity was taken to refly the Oxford equipment with more involvement by the Meteorological Office. This was opportune since a new White cell facility had been set up at the Meteorological Office to measure the stratospheric sounding units spectral response.

The purpose of this note is to record the results of the 17 March 1976 flight and compare these results with the laboratory measurements and theoretical calculations done by the Meteorological Office.

While the previous problems were overcome, there were new difficulties. Soon after launch the recorded data became erratic and the decommutation required a major computational effort (by B.B.). (The problem was aided by the early failure of the NOAA spectrometer which provided low readings in alternative channels, and hence could be used as a basic synchronization indicator). The precision of the final comparison between calculation and flight transmission results is limited by

a. the pressure tranducer uncertainty of .3 mb,

b. the uncertainty of the absolute calibration and gain stability of the pressure modulation channel,

c. the apparent fluctuation of the sun signal as monitored by the window channel.

Following a brief explanation of the technique for measuring atmospheric attenuation and a description of the apparatus, the results of laboratory White cell measurements and the balloon flight will be presented.

2. The balloon experimental concept and design details

The detailed design and concept of the balloon experimentation are described in Dr Delderfield's thesis (q.v.). A brief description of the method and the salient features of the optical and spectrally sensitive parts is presented here.

The basis of the experiment is to monitor the radiance received from the sun in the spectral passband of the sounding radiometer as the balloon ascends. One of the problems with such a measurement is the inability of making direct observations with and without the atmosphere (the ratio being the transmission) as the balloon ascends. Even at the balloon ceiling of $\sim$40 km there is residual absorption in the pressure modulator channel of .16. In order to monitor the sun signal as received through the optics system a window channel is included; also to enable scaling to absolute transmission a wideband signal is generated. The use of these channels to establish a transmission profile is described in section 4.

Figure 1 (Figure 4.2 of Delderfield 1977) is a simplified optics schematic. The solar beam illuminates the scatter plate (which can rotate about an axis perpendicular to the paper); this acts as a plane mirror at the wavelengths (11-15 μ m) of interest. The solar beam is reflected on to the main mirror A, which forms part of a telescope focusing the solar image at B. These two mirrors can rotate about the axis 'A-spectrometer input'. Rotation about these two axes is servo driven, by a sunseeker arrangement. The flip mirror is moved, about every two minutes, between B and C so that the mirror M1, the first component of the PM system, views the sunseeker radiation for 2 minutes, then views the blackbody D for a different 2 minute period; this sequence repeats throughout the flight.

The long lightpipe acts as an image scrambler to remove jitter caused by servo delays and inhomogenuities in the fore optics. Figure 2 (Figure 4.7 of Delderfield 1977) details the optical arrangement beyond this lightpipe. The view of the pressure modulator channel is time multiplexed, by the reflective chopper, between a 'direct' view of the transmitted solar beam and a reflected view of an internal black body.

A complimentary 12 μm 'window' channel is also chopped by the reverse side of the reflective 'bow tie' chopper so as to directly view the internal blackbody and to reflectively view the solar beam. The chopper modulates the window channel at 400 Hz. The same modulation of 400 Hz for the pressure modulated channel is also beating with pressure modulation of the gas (carbon dioxide at $\sim$75 torr) in the gas cell. Three signal frequencies are extracted from the pressure modulated channel detector:

a. The signal at 400 Hz, which is phase sensitive detected and integrated for 1s. This is the equivalent of averaging out the pressure modulator variation to give a signal with spectral dependence due to the characteristics of the bandpass filter modified by a 1 cm cell with a mean pressure of 75 torr. This channel is termed the "wide band" signal (WB).

b. The sideband signal, which is derived by detecting and integrating the pressure modulator ripple on the 400 Hz output. This signal proved to be noisy - presumably due to chopper jitter and was not used in the measurements.

c. The signal at the pressure modulation frequency - this is phase sensitive detected and integrated over 1s. This is the slow chop or pressure modulated signal and is the mean of the solar beam and internal black body radiances chopped by the varying gas absorption due to the pressure cycle. This signal (PM) is equivalent to that generated in the Met Office stratospheric sounding unit when viewing the atmosphere.

The absolute ground based calibration, though repeatable, proved unreliable due to inadequate flushing to remove residual carbon dioxide from the reference target used. Hence the need for the wideband signal as a method of estimating the solar intensity at 15 μm outweighs the loss of a factor of 2 in the pressure modulated signal level due to the chopping at 400 Hz. This method is also convenient to beam split for the window channel (which needs a chopper).

The window channel allows monitoring of any variations of the sun signal which, while common to the wideband and pressure modulated signals, are not due to the atmosphere (the time constant problem is discussed in Section 4).

For completeness Figure 3 is a block diagram of the flight apparatus.

Three input conditions to the PM box were monitored during the flight, viz

a. Sun: this is with the scatter plate and sunseeker orientated such that the solar image enters the PM box (Figure 1);

b. Sky: the scatter plate is tilted off the sun by $\sim 2^{\circ}$ so that the signal is due to atmospheric emission;

c. Black Body: the black body signal is the radiation measured when the 'Flip mirror' has moved to position C (see Figure 1).

3. Weighting Function runs

As part of the Met Office experimental support work for the Tiros N SSU, routine measurements are made of the weighting functions for the pressure modulators used in these stratospheric Sounding Units. This work has already been described (e.g. Pick 1976). The necessary modifications to record data and optically interface to the Oxford balloon flight system were done. This enabled the transmission through a uniform pressure path (simulating an atmospheric path of carbon dioxide) to be measured with the pressure modulator and chopper configuration of Figure 2 in the same orientation as during flight and at the same nominal thermostated temperature (35°C). The table lists the relevant conditions for the measurement runs made (for a definition of terms, see Annex A). The PM frequency was used to infer mean cell pressure.

Table 1

Run	Date	Tank	Parameters	Cell p(mb)	PM/WB	Comment
OXO	29/1/76	l=9.116m	C=0.2868 T=20.0°C	102.1	.799±.002	Preflight
OXP	1/4/76	"	C=0.2881 T=20.5°C	103.6	.827±.002	Post flight runs
OXQ	2/4/76	"	C=1 T=22.3°C	103.8	.822±.002	Pure CO_2
OXR	5-6/4/76	"	C=.2887 T=-12°C	104.2	.825±.003	Cold run
OXS	7/4/76	"	C=.2905 T=19.9	104.2	.829±.004	
OXT	8/4/76	"	C=.2917 T=28.3	104.2	.835±.002	No lens
	17/3/76	Flight		102.0	.799±.002	

Annex A details the transmission measurements and the theoretical calculation results (see Section 4) for the particular conditions of the tank parameters and the PM mean pressure. The differences between calculated and measured transmissions are plotted in Figures 4 to 8, while Figure 9 indicates the expected differences for a 10% increase in the mean pressure inside the PM. The figure shows that a systematic error in the cell pressure gives an omnidirectional error, with a maximum deviation at about $\gamma = 0.5$. However the wide band transmission difference is about 10 times less sensitive than the PM difference. Also on Figure 4 is plotted the mean systematic difference between theory and experiment for all runs. The effect of correcting for the spectral shape of the hot source is also shown in Figure 4. It decreases the differences by .003 for the wideband case but has negligible effect on the pressure modulator curve. The error bars are mainly caused by a reproducibility problem of the pre and post run zero pressure scaling factors. This manifests itself as variation in White cell/bypass ratio. Typically the difference between five consecutive measurements was $\sim$ .1%, but the variation between start and finish in the worst case was $\sim$ 4%, with no obvious sudden change during the run. Table 2 details this ratio for the various runs.

Table 2 White cell/Bypass ratio

	Wideband		Pressure Modulator	
	Pre	Post	Pre	Post
OXO	$.465 \pm .002$	$.465 \pm .002$	$.464 \pm .003$	$.467 \pm .003$
OXP	$.5605 \pm .0003$	$.5446 \pm .0007$	$.563 \pm .001$	$.544 \pm .005$
OXQ	$.5473 \pm .0006$	$.5445 \pm .0007$	$.543 \pm .004$	$.545 \pm .003$
OXR		$.5783 \pm .0009$		$.575 \pm .003$
OXS	$.5616 \pm .0007$	$.5434 \pm .0006$	$.563 \pm .0006$	$.563 \pm .009$
OXT	$.5644 \pm .0007$	$.5635 \pm .0006$	$.568 \pm .004$	$.566 \pm .002$

(The standard deviation quoted is derived from the variation in the 5 samples used to measure this ratio).

A systematic difference of this shape and size shown in figure 4 will give radiance errors equivalent to $\sim$ .4, .3 and .2°K for the low pressure (1.5 mb), medium pressure (5mb) and high pressure cells (15 mb) of the SSU.

Figure 10 plots the ratio of PM/WB for the full scale signals with the estimated cell pressure under the measurement conditions using the pressure versus frequency information given in Delderfield's thesis. This number is useful for scaling the sky/sun difference to a transmission value.

4. Flight results

The conversion of the SUN-SKY signal to a transmission table as a function of pressure and sun angle relies on a knowledge of:

a. Variations in sun signal due to obstructions in optics field of view and wobble of the sun image;

b. Gain change or constancy of gain;

c. Full scale signal values;

d. Balloon pressure altitude and location (as a function of time) and atmospheric conditions:

4.1 Constancy of the sun signal

The prime indicator of constancy of the sun signal is the output of the window channel since the atmospheric attenuation is expected to be below 1% at 300 mb and negligible above 100 mb. During ascent for a particular value of pressure, the reading and its standard deviation (obtained from an average of about 20-30 successive ramp readings) showed that the standard deviation for the sun reading was larger than the value for the sky or blackbody signal and the successive average values of the window sun signal varied by $\sim$ 1-2%. Figure 11 demonstrates the problem in more detail. This change is larger than that due to the decrease in atmospheric attenuation. While the time response of the PM channel is longer than either the window channel or the WB signal the small size of the effect allows rescaling of PM and WB by the change in window channel signal. This jump must be associated with the alignment servo system which rotates the sunseeker to follow the sun. Hawser crossing problems (not seen on this flight) cause a much larger signal dropout. If the window channel signal were to be used to rescale for difference of a larger size, then the time response differences would need to be taken into account (by numerical filtering of the window channel). This has not been done in this instance.

4.2 Gain change or constancy of gain

The inflight calibration is difficult to assess because only one black body reference signal level is measured and it is much smaller than the sun signal; further this black body signal varied much faster than the change in radiance due to changes in the black body temperature: Hence a scheme had to be devised to separate offset changes (which are unimportant due to subtraction of the sky signal from the sun signal) from any gain changes. Annex B lists housekeeping monitors. It is apparent that for critical temperatures (those which are likely to affect the gain) above 70 mb during ascent the temperatures remained constant to $\sim \frac{1}{4}^{\circ}$C. Hence if it can be shown that the gain is sensibly constant during float, there is some confidence in assuming constancy of gain during ascent. Also the sky radiation signal is easier to estimate at float since it has a smaller value and hence larger proportional error tolerance.

In Annex C an expression of the response of a channel is derived as:

$$G = \underbrace{(V_{sky} - V_{BB})}_{\text{signal difference}} \Big/ \underbrace{(r_{ms} R_{sky}}_{\text{sky emission}} + \underbrace{(1-r_{ms}) R_{ms}}_{\text{optics emission}} - \underbrace{R_{BB})}_{\text{External black body}}$$

Figure 12 shows the window signals, the x are the cubic spline fit. The derived response values G are plotted in figure 13. The variation for the window channel gain of $\sim$ 4% indicated by the $\mathbf{I}$ in Figure 13 is equivalent to the (1) in Figure 12: hence the method is inadequate to determine that the gain is constant to .25%, though it does show that the major change in counts output for the two signals over the interval shown in Figure 12 is a change in offset.

4.3 Full scale signal values

Assuming constancy of the gain during the flight Table 3 is derived for different optics assumptions

Table 3

Estimate of response G (counts/sec)/(m $W/m^2 s$ r cm^{-1})

$r_m r_s$	$T_{m/s}$	G_{PM}	G_{WB}	G_{11}	PM/WB	WB/11 μ
.87	270K	$1.362 \pm .007$	$1.745 \pm .008$	$.791 \pm .005$	$.780 \pm .006$	$2.21 \pm .02$
.87	250K	$1.339 \pm .007$	$1.716 \pm .008$	$.776 \pm .008$	$.779 \pm .006$	$2.24 \pm .02$
1	250K	$1.291 \pm .008$	$1.638 \pm .008$	$.716 \pm .004$	$.758 \pm .006$	$2.29 \pm .02$

The atmospheric transmissions, listed in Annex D and shown in Figure 15, were derived assuming a ratio of $.785 \pm .004$ (PM/WB of Table 1 and included α of Annex C) and τ_{top} for the wideband signal of .955 at block 277 as detailed in Annex C.

4.4 Balloon pressure altitude and location (as function of time,) and atmospheric conditions.

The pressure profile is derived from three pressure tranducers which were switched at 134 mb and 16 mb. These tranducers were calibrated before the flight and the middle pressure (134-16 mb) unit was recalibrated after recovery. The quoted accuracies were ± 5 mb, ± 1 mb and $\pm .3$ mb. However, the low pressure end values were adjusted to give a smooth transition to the high pressure end of the next gauge. Radar was used to locate the balloon and the sun angle calculated from an ephemeris. The sonde data are plotted in Figure 14.

4.5 Theoretical calculation

A Drayson (1965, 1966) line by line programme using a Voigt line profile and McClatchey line data (1975) was modified to run with a pressure modulator; this programme was used to generate a table of atmospheric transmission at 35 standard levels for nominal, cell pressure and "nominal + 10%" cell pressure and several sun angles, at 1 cm^{-1} intervals. This is the technique which has been adopted for the SSU weighting function. A spot reading is obtained by:

a. convolving the table with the measured filter profile;

b. interpolating the table to the effective mean cell pressure (from laboratory weighting function measurements);

c. logarithmically interpolating between adjacent pressure levels;

d. interpolating to the required angle by using the secant of the angle;

The systematic offsets measured during the laboratory measurements have been included in deriving Figure 16. This fit is satisfactory for the pressure modulator channel as shown in Figure 16 while the wide band channel shows a large $\sim .03$ systematic difference. This difference is opposite to the systematic difference between theory and measurement found for the weighting function difference. The cause of this discrepancy is unresolved.

5. Conclusion

The flight has demonstrated that the calculation of atmospheric transmission function for the high pressure modulator is within the experimental accuracy of measurement. However the uncertainty due to scaling, the pressure transducer calibration and possible gain changes are large ($\sim$ 0.02 near full scale) compared with inaccuracy of about 0.003 in atmospheric transmission profile required to make the radiance error from the atmosphere equal to the SSU instrumental noise. Hence a reflight of the balloon experiment without improvement in these areas is not recommended.

6. Acknowledgements

The main experimental effort and design of the balloon experiment was a joint exercise between NESS of NOAA and Oxford University. J.Delderfield of Oxford designed and integrated the pressure modulator and window channel electronics into NOAA's p.m.r. box. The sunseeker and data logging system were provided by Denver University. Dr.L.Stowe of NESS managed the NOAA effort and supervised the integration. In house weighting function measurements were supported by D.E.Warner. The United States Air Force provided the balloon launch and recovery facilities.

7. References

J.J.Batey, 1975 D.Phil. thesis Oxford University.

H.E.Bennett, 1963 J. Opt. Soc. Amer. 53 p 1389.

J.Delderfield, 1977 D.Phil. thesis Oxford University.

S.R.Drayson, 1965 NASA Technical Note D2744.

S.R.Drayson 1966 Appl. Optics 5, p 385.

M.F.Kimmit 1970 Far-Infrared Techniques.

D.R.Pick, D.E.Warner, P.Kent and R.D.Carter 1976 SSU Tech. Comm. 98 (Met Office internal note).

Annex A

Table of comparison between experimental weighting function runs on the Oxford balloon flight modulator and chopper system and spectral transmission calculations

PM - signal measured at modulator frequency
WB - wideband signal - chopper frequency
l - pathlength in tank always 9.116 m
c - pressure mixing ratio $CO_2/(CO_2+N_2)$
f - frequency of pressure modulation Hz
p - pressure (mean) inside pressure modulator optical cell, mb

Run	OXO	c=0.2868 measured transmission		f=53.53±.03 Hz line by line calculation		p=102.1±.1 mb CAL - MEAS	
Tank Gas press	Tank Gas Temp	PM	WB	PM	WB	PM	WB
1.97	20.8	.913	.979	.922	.976	.009	-.003
3.75	20.7	.813	.958	.823	.954	.010	-.003
7.11	20.6	.635	.923	.641	.907	.006	-.005
9.80	20.5	.524	.874	.526	.867	.003	-.007
13.50	20.4	.410	.822	.409	.813	.001	-.009
18.61	20.4	.304	.752	.300	.741	-.004	-.011
25.64	20.3	.213	.664	.208	.652	-.005	-.012
35.33	20.2	.140	.560	.135	.546	-.005	-.014
48.66	20.0	.084	.443	.080	.428	-.004	-.014
92.36	19.8	.021	.213	.020	.202	-.002	-.012
175.33	19.6	.004	.077	.003	.068	-.001	-.010
332.94	19.5	.001	.026	.000	.019	-.002	-.007

PM/WB is measured for zero pressure in tank (White cell) as simple counts ratio for a particular view minus offset.

Run	OXP	C=0.2881		f=58.86±.03Hz		p=103.6±.1 mb	
Tank gas P	Tank gas T	measurement PM	WB	line by line calculation PM	WB	CAL-MEAS PM	WB
.50	21.8	.977	.994	.983	.992	.006	.010
1.82	21.5	.914	.978	.931	.978	.018	.001
3.48	21.3	.825	.958	.841	.958	.016	-.004
6.65	21.1	.652	.915	.667	.913	.015	-.001
9.20	21.0	.542	.878	.553	.876	.011	-.002
12.71	20.9	.428	.827	.435	.824	.007	-.003
17.58	20.8	.320	.760	.322	.755	.002	-.005
24.31	20.8	.227	.674	.225	.668	-.002	-.006
44.98	20.6	.098	.463	.093	.457	-.005	-.006
64.23	20.5	.052	.332	.047	.324	-.004	-.009
122.76	20.3	.011	.134	.008	.127	-.002	-.007
234.71	20.2	.001	.045	.001	.039	.000	-.006

Run	OXQ	C=1.000		f=53.89±.03		p=103.8±.1 mb	
Tank gas P	Tank gas T	measurement PM	WB	line by line calculation PM	WB	CAL - MEAS PM	WB
.95	22.5	.915	.973	.919	.973	.004	-.001
1.82	22.4	.816	.952	.821	.950	.005	-.003
3.48	22.3	.645	.907	.637	.900	-.008	-.007
4.82	22.3	.534	.865	.521	.858	-.013	-.007
6.68	22.2	.417	.812	.402	.800	-.015	-.012
9.24	22.2	.307	.741	.292	.725	-.014	-.016
12.80	22.2	.211	.649	.199	.631	-.012	-.019
17.72	22.2	.134	.542	.126	.520	-.008	-.022
24.54	22.2	.080	.423	.073	.400	-.007	-.023
47.03	22.2	.018	.195	.016	.177	-.002	-.018
90.16	22.2	.004	.067	.002	.056	-.002	-.011

Run	OXR	C=.2887		f=53.98±.03		p=104.2±.1 mb	
Tank gas P	Tank gas T	measurement PM	WB	line by line calculation PM	WB	CAL - MEAS PM	WB
2.46	-16.3	.896	.976	.898	.974	.014	-.002
4.38	-16.1	.775	.953	.783	.950	.008	-.003
7.80	-16.0	.600	.904	.601	.901	.002	-.003
10.41	-15.9	.500	.866	.497	.863	-.003	-.004
13.89	-15.8	.401	.816	.394	.812	-.007	-.004
18.55	-15.6	.310	.750	.299	.747	-.011	-.003
24.77	-15.4	.228	.671	.216	.668	-.011	-.003
44.16	-15.0	.103	.478	.096	.471	-.011	-.007
78.81	-14.4	.033	.268	.031	.261	-.002	-.006
140.67	-13.7	.007	.122	.006	.115	-.001	-.008
251.22	-12.9	.004	.052	.001	.045	-.002	-.007
448.63	-12.1	.002	.019	.000	.014	-.002	-.004

Run	OXS	C=.2905		f=54.00		p=104.3±.1	
Tank gas P	Tank gas T	measurement		line by line		CAL - MEAS	
		PM	WB	PM	WB	PM	WB
1.83	23.1	.917	.979	.930	.978	.014	-.001
3.49	22.8	.833	.959	.841	.957	.008	-.002
6.68	22.5	.657	.914	.666	.913	.010	-.002
9.23	22.4	.545	.877	.553	.875	.007	.003
12.76	22.1	.430	.827	.434	.823	.004	-.005
17.64	21.9	.322	.760	.321	.753	-.001	-.007
24.40	21.8	.229	.674	.224	.666	-.005	-.008
46.64	21.4	.095	.453	.087	.442	-.008	-.012
86.31	21.0	.029	.230	.023	.220	-.005	-.010
170.09	20.0	.002	.078	.003	.071	.001	-.008
324.92	19.4		.026	.000	.020		-.006

Run	OXT	C=0.2917		f=53.98±.04H$_2$		p=104.2±.1 mb	
Tank gas P	Tank gas T	measurement		line by line		CAL - MEAS	
		PM	WB	PM	WB	PM	WB
1.54	27.6	.932	.982	.943	.980	.011	-.001
2.99	27.5	.857	.965	.869	.963	.012	-.002
5.68	27.5	.703	.928	.740	.932	.015	.004
8.08	27.5	.600	.895	.602	.891	.002	-.005
11.25	27.5	.485	.850	.481	.843	-.004	-.006
15.66	27.5	.369	.789	.362	.779	-.007	-.009
21.81	27.5	.262	.707	.256	.696	-.007	-.010
40.92	27.5	.115	.501	.108	.488	.007	-.013
82.97	27.6	.031	.244	.026	.234	-.004	-.010
159.21	27.7	.005	.085	.003	.076	-.002	-.008
309.07	28.0	.002	.026	.000	.021	-.002	-.006
600.6	28.6	.001	.007	.000	.004	-.001	-.003

Annex B

Table of Housekeeping Monitors

Block	50	100	150	200	250	300	900	
Ambient Pressure mb	191.5	70.2	28.6	12.4	6.40	4.53		
PM filter	35.9	35.9	35.9	35.9	36.0	35.9	36.4	°C
PM detector	36.0	36.0	36.0	36.0	36.0	36.0	36.4	
PM preamp	35.9	35.9	35.9	35.9	35.8	36.0	36.5	
PM cell	35.9	35.7	35.4	35.2	35.4	35.4	37.3	
11μm filter	36.0	36.0	36.0	35.9	35.9	35.9	36.2	
11μm detector	36.3	36.3	36.3	36.3	36.4	36.3	36.4	
11μm preamp	35.2	35.1	35.0	35.0	35.0	35.0	35.4	
lightpipe	33.8	32.7	32.3	32.3	32.4	32.8	35.5	
chopper shroud	35.4	32.5	31.3	30.7	30.8	31.1	38.5	
Ref BB	30.4	35.4	35.5	35.5	35.5	35.5	35.8	
Baseplate	32.9	31.1	29.6	29.0	29.2	29.6	35.8	
Sun L degrees	37.3	35.0	33.9	33.7	34.6	36.7		

Housekeeping zero off scale due to component failure

ANNEX C

Relationship between outputs and radiation incident on the flip mirror

Symbols

V output signal counts/s

Vo offset "

G the response of the system to radiance incident on the flip mirror (Figure 1) within the field of view of the instrument (counts/s)/(mW/m^{2}sr cm^{-1})

τ_{atm} transmission between sun and scatterplate

R radiation mW/m^{2}sr cm^{-1}

R_{sun} solar energy incident on scatterplate

($R = \int f_\nu B(\nu,T)\, d\nu / \int f_\nu d\nu$ where f_ν is the spectral response of the instrument, $B(\nu,T)$ the appropriate Planck function at wavenumber ν and temperature T K)

R_{sky} radiation from sky emission incident on the scatterplate

R_M radiation from main mirror (emissivity not included)

R_S radiation from scatterplate (")

R_{BB} radiation incident on Flip mirror from the reference black body

r_m reflectivity of main sunseeker mirror

r_s reflectivity of scatterplate

Note: these are all channel dependent ie. vary with spectral position

Hence we can write for each channel

$$V_{sun} = G(((\tau_{atm} R_{sun} + R_{sky})r_s + (1-r_s)R_s)r_m + (1-r_m)R_m) + V_o$$

$$V_{sky} = G((R_{sky} r_s + (1-r_s)R_s)r_m + (1-r_M)R_m) + V_o$$

$$V_{BB} = G R_{BB} + V_o$$

and the offset is eliminated by taking differences hence

$$G = (V_{sky} - V_{BB})/((R_{sky} r_s + (1-r_s)R_s)r_m + (1-r_m)R_m - R_{BB})$$

where $r_{ms} = r_m \times r_s$ and $R_{Ms} = R_M = R_s$

$$G = (V_{sky} - V_{BB})/(r_{ms} R_{sky} + (1-r_{ms}) R_{ms} - R_{BB})$$

and $$\tau_{atm} = \frac{V_{sun} - V_{sky}}{G\, R_{sun}\, r_m r_s}$$

The various terms in the expression can be measured, ratioed or estimated as detailed below.

r_m, r_s The main mirror is a front aluminized mirror, while the scatterplate is an aluminized ground glass reflector. Bennett (1963) has given an expression for the reflectivity ratio of

$$r_s = r_m \exp\left(-\left(\frac{4\pi\sigma}{\lambda}\cos\psi\right)^2\right).$$

where $4\pi\sigma$ is a roughness factor, measured by the variation of r_s with ψ to be $3.77 \pm .07\,\mu m$. During ascent the angle of incidence was approximately constant at 18° (half sun angle).

Bennett's expression yields the following values for $r_m r_s$ using the values of r_m for aluminized mirror given in Kimmit (1970)

	$\psi = 10$	$\psi = 20$	$\psi = 30$	r_m
11 μm	.862	.870	.885	.983
15 μm	.914	.919	.926	.985

R_{sky} This can be estimated in the usual way from the radiative transfer equation as

$$R_{sky} = \int_{\text{Balloon at } z}^{\text{top}} \int_\nu f(\nu) B_\nu(T_{z'}) \frac{d\tau_{z'-z}}{dz'} dz' d\nu \Big/ \int_\nu f(\nu)\, d\nu$$

where z' includes the "sun angle"

R_{ms} The previous flight in which the optics temperature was measured gave a T of 250–270 K. A very approximate thermal analysis indicates this is not unreasonable.

The magnitude of the various terms during the float phase are thus

	Pressure Modulator	Wide Band	12 μm Window	
R_{BB}	123 – 147	124–148	104–129	$\frac{mW}{m^2\,sr\,cm^{-1}}$
$r_{ms} R_{sky}$	10 – 15	1.5–1.6	0	
$(1-r_{ms})R_{ms}$	8 – 12 (250K mirror / 270K mirror)	8–12	9–13	

Because of the uncertainty in the optics term which is about 10% of R_{BB}, the estimation of the scaling to find the atmospheric transmission is carried out as follows; assume $(\tau\ \text{top})_{WB}$ is known (.955)

hence $$(R_{sun})_{WB} = \frac{(V_{sun} - V_{sky})_{WB}}{\tau_{top}\,(G r_m r_s)_{WB}}$$

and define α_s such that

$$(R_{sun})_{PM} = \alpha_s (R_{sun})_{WB} = \frac{(V_{sun} - V_{sky})_{PM}}{(\tau_{atm})_{PM}\,(G\, r_m r_s)_{PM}}$$

$$\text{hence } (\tau_{atm})_{PM} = \frac{(V_{sun} - V_{sky})_{PM}}{(V_{sun} - V_{sky})_{WB\ top}} \cdot \frac{1}{\alpha_s} \cdot \frac{(G\, r_m r_s)_{WB}}{(G\, r_m r_s)_{PM}} \cdot (\tau_{top})_{WB}$$

but r_m and r_s change slowly with wavelength; α_s is easily found by assuming the sun is a black body at 5785K and convolving with the filter profile (for the WB) and the pm "chopping profile" (for the PM); G_{WB}/G_{PM} is measured during weighting function runs or as derived above; (Note an α_w and α_B are required for the weighting function source and the flight reference black body, values of

$\alpha_s = .983$; $\alpha_w = .989$; and $\alpha_B = 1.004$ were calculated)

$(\tau_{top})_{WB}$ is insensitive to pressure errors and the value is estimated from the weighting function runs.

ANNEX D

TABLE OF FITTED TRANSMISSION FOR BALLOON

SCALE -0.5722 SYM ERR REMOVED OZONE CORR

BLOCK	P MB	ANG	PM	WB	PM +	WB+						Measured PM	Measured WB	CAL-OBS PM	CAL-OBS WB
25	356.94	38.9	0.0027	0.0717	0.0030	0.0724	0.0026	0.0713	0.0026	0.0761	0.0026	0.0736	.005	.067	-.002	.007
41	247.21	37.9	0.0076	0.1287	0.0083	0.1297	0.0072	0.1280	0.0074	0.1360	0.0071	0.1318	.011	.119	-.004	.012
57	158.85	36.9	0.0202	0.2109	0.0220	0.2126	0.0192	0.2100	0.0196	0.2186	0.0190	0.2124	.020	.192	-.001	.020
79	104.54	35.6	0.0477	0.3254	0.0519	0.3279	0.0453	0.3240	0.0462	0.3334	0.0451	0.3254	.051	.295	-.006	.030
101	68.99	34.9	0.0978	0.4668	0.1062	0.4700	0.0931	0.4649	0.0949	0.4743	0.0931	0.4651	.098	.430	-.005	.035
119	50.39	34.4	0.1535	0.5758	0.1662	0.5794	0.1463	0.5736	0.1492	0.5819	0.1469	0.5728	.150	.543	-.004	.033
143	32.59	33.9	0.2595	0.7068	0.2792	0.7107	0.2483	0.7046	0.2532	0.7116	0.2501	0.7028	.249	.684	.001	.018
149	29.20	33.9	0.2897	0.7365	0.3111	0.7404	0.2774	0.7342	0.2814	0.7409	0.2782	0.7323	.279	.716	-.001	.016
159	24.65	33.8	0.3410	0.7766	0.3650	0.7804	0.3273	0.7744	0.3296	0.7807	0.3268	0.7739	.327	.761	.000	.013
167	21.29	33.6	0.3838	0.8068	0.4143	0.8104	0.3739	0.8047	0.3748	0.8106	0.3720	0.8046	.375	.796	-.003	.008
175	18.66	33.6	0.4331	0.8314	0.4606	0.8348	0.4173	0.8295	0.4167	0.8346	0.4141	0.8294	.418	.821	-.004	.008
181	17.04	33.6	0.4643	0.8469	0.4928	0.8501	0.4480	0.8451	0.4464	0.8497	0.4439	0.8449	.451	.844	-.007	.001
189	15.13	33.7	0.5056	0.8653	0.5349	0.8684	0.4833	0.8636	0.4858	0.8677	0.4834	0.8635	.488	.857	-.005	.006
197	13.04	33.7	0.5577	0.8860	0.5876	0.8888	0.5406	0.8843	0.5359	0.8878	0.5337	0.8842	.535	.880	-.001	.004
207	11.11	33.8	0.6124	0.9035	0.6416	0.9059	0.5956	0.9021	0.5891	0.9050	0.5870	0.9019	.589	.904	-.002	-.002
219	9.17	33.9	0.6754	0.9221	0.7033	0.9241	0.6595	0.9209	0.6508	0.9233	0.6491	0.9208	.650	.924	-.001	-.004
225	8.71	34.0	0.6915	0.9263	0.7188	0.9282	0.6758	0.9251	0.6666	0.9274	0.6649	0.9251	.663	.926	.002	-.001
235	7.64	34.2	0.7308	0.9362	0.7565	0.9379	0.7151	0.9352	0.7061	0.9372	0.7046	0.9352	.701	.937	.004	-.002
241	6.95	34.4	0.7570	0.9423	0.7812	0.9438	0.7432	0.9414	0.7332	0.9431	0.7313	0.9414	.723	.944	.009	-.003
251	6.32	34.6	0.7819	0.9479	0.8045	0.9492	0.7690	0.9471	0.7590	0.9487	0.7577	0.9471	.752	.946	.006	.001
259	5.89	34.8	0.7980	0.9512	0.8193	0.9525	0.7858	0.9505	0.7758	0.9520	0.7746	0.9506	.772	.942	.003	+.008
275	5.32	35.5	0.8208	0.9560	0.8403	0.9571	0.8096	0.9554	0.7996	0.9567	0.7936	0.9555	.795	.955	.004	.000
283	5.07	35.8	0.8315	0.9583	0.8502	0.9593	0.8209	0.9577	0.8109	0.9589	0.3099	0.9578	.804	.958	.006	.000
289	4.81	36.1	0.8415	0.9603	0.8592	0.9613	0.8314	0.9597	0.8214	0.9609	0.8206	0.9599	.812	.959	.008	.001
297	4.67	36.4	0.8465	0.9612	0.8637	0.9622	0.8367	0.9607	0.8267	0.9619	0.8258	0.9609	.822	.962	.004	-.001
313	4.25	37.1	0.8630	0.9645	0.8785	0.9654	0.8541	0.9640	0.8441	0.9651	0.8434	0.9643	.833	.966	.010	-.002
345	4.21	38.6	0.8629	0.9644	0.8785	0.9653	0.8541	0.9639	0.8441	0.9650	0.8434	0.9642	.840	.974	.003	-.010
361	4.25	39.4	0.8620	0.9633	0.8758	0.9647	0.8510	0.9633	0.8410	0.9644	0.8403	0.9636	.838	.972	.002	-.009
371	4.24	40.1	0.8596	0.9637	0.8755	0.9646	0.8505	0.9632	0.8405	0.9643	0.8399	0.9635	.835	.972	.005	-.009
391	4.25	41.4	0.8573	0.9632	0.8734	0.9640	0.8481	0.9627	0.8381	0.9638	0.8374	0.9630	.838	.976	-.003	-.013
401	4.26	42.0	0.8559	0.9623	0.8721	0.9637	0.8466	0.9623	0.8366	0.9635	0.8359	0.9627	.828	.964	.016	-.001
434	4.27	44.5	0.8512	0.9618	0.8679	0.9627	0.8417	0.9612	0.8317	0.9624	0.8310	0.9616	.821	.967	.010	-.005
459	4.27	45.7	0.8492	0.9613	0.8660	0.9622	0.8395	0.9607	0.8295	0.9619	0.8288	0.9611	.816	.971	.012	-.010
469	4.26	46.9	0.8476	0.9609	0.8645	0.9618	0.8378	0.9603	0.8278	0.9615	0.8272	0.9607	.806	.967	.019	.006
502	4.63	50.0	0.8238	0.9553	0.8429	0.9569	0.8129	0.9551	0.8029	0.9565	0.8021	0.9556	.785	.964	.017	.009
520	4.86	51.6	0.8098	0.9527	0.8301	0.9539	0.7981	0.9520	0.7881	0.9535	0.7873	0.9525	.770	.966	.017	.014
540	5.15	53.4	0.7909	0.9485	0.8127	0.9498	0.7785	0.9478	0.7685	0.9493	0.7676	0.9482	.740	.942	.028	.008
560	5.54	55.2	0.7652	0.9425	0.7887	0.9440	0.7518	0.9417	0.7418	0.9434	0.7408	0.9422	.713	.931	.027	.011
584	6.00	57.5	0.7350	0.9353	0.7602	0.9369	0.7206	0.9343	0.7106	0.9363	0.7095	0.9349	.679	.918	.030	.016
614	6.65	60.4	0.6920	0.9244	0.7194	0.9263	0.6764	0.9233	0.6672	0.9256	0.6660	0.9239				

"Includes sun profile"

Coln 1 Block count. 2 Balloon pressure altitude mb (± .25 mb). 3. Calculated solar angle (from zenith) for balloon location, height and time. (4 and 5 line by line calculation for mean cell pressure 108.2 mb, 5 and 6 ditto p = 119.0) for conditions given including sun as BB. 7 and 8 Weighting for systematic error removed. 9 and 10 ozone correction included. 11 and 12 measured values 13 and 14 difference - calculation -- observation.

SIMPLIFIED OPTICS SCHEMATIC FIGURE 1.

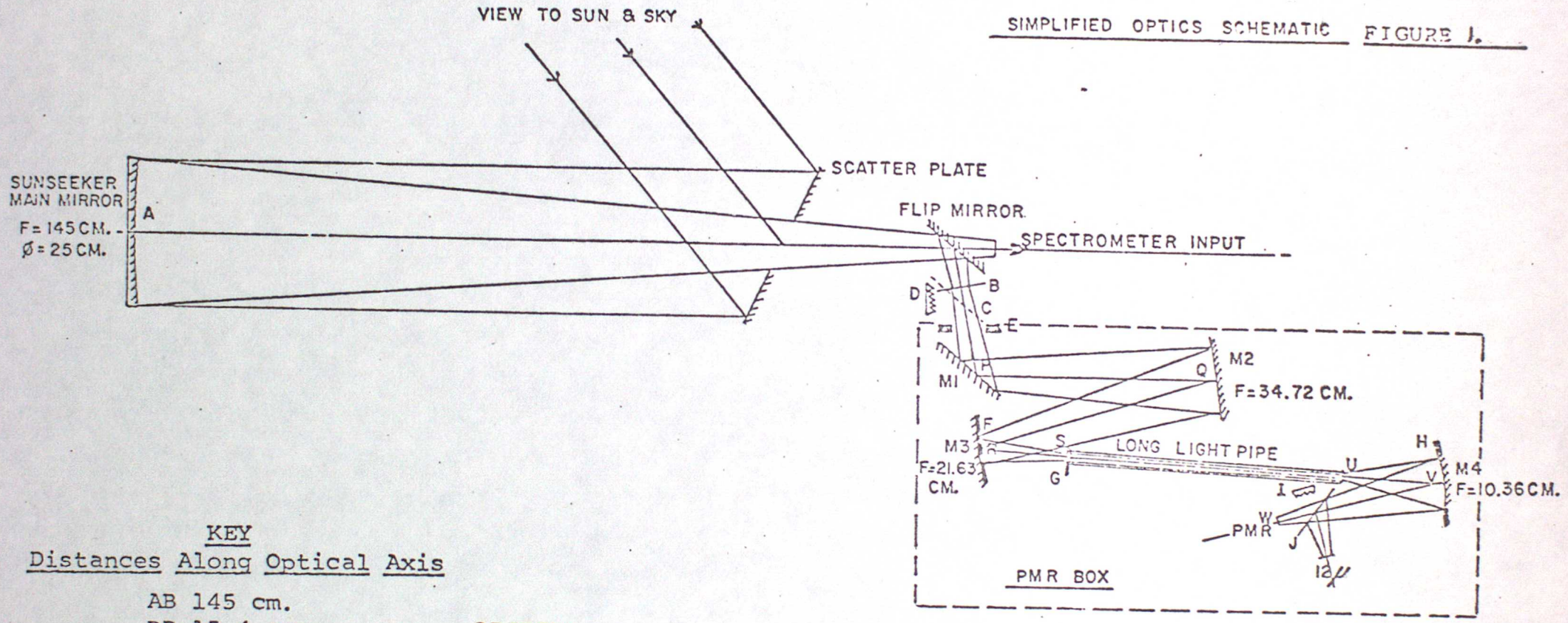

KEY

Distances Along Optical Axis

AB 145 cm.
BP 15.4 cm.
PQ 40 cm.
QR 42 cm.
RS 15.19 cm.
UV 16 cm.
VW 29.39 cm.

OBJECTS

B. Sun's image made by sunseeker main mirror.
C. Alternative position of flip mirror.
D. Black body which radiometer sees in position C.
E. Stop outside field of view to keep the sun out of the box in the sky view position.
F. Aperture stop - thermostatted & focused on sunseeker main mirror.
G. Field stop - thermostatted & focused on B.
H. Stop to remove tails on Ge lens field of view from PMR & 12μ.
J. Reflective chopper.
I. Thermostatted black body.

P.M. & 12μ CHANNEL OPTICAL INTERFACE

FIGURE 2.

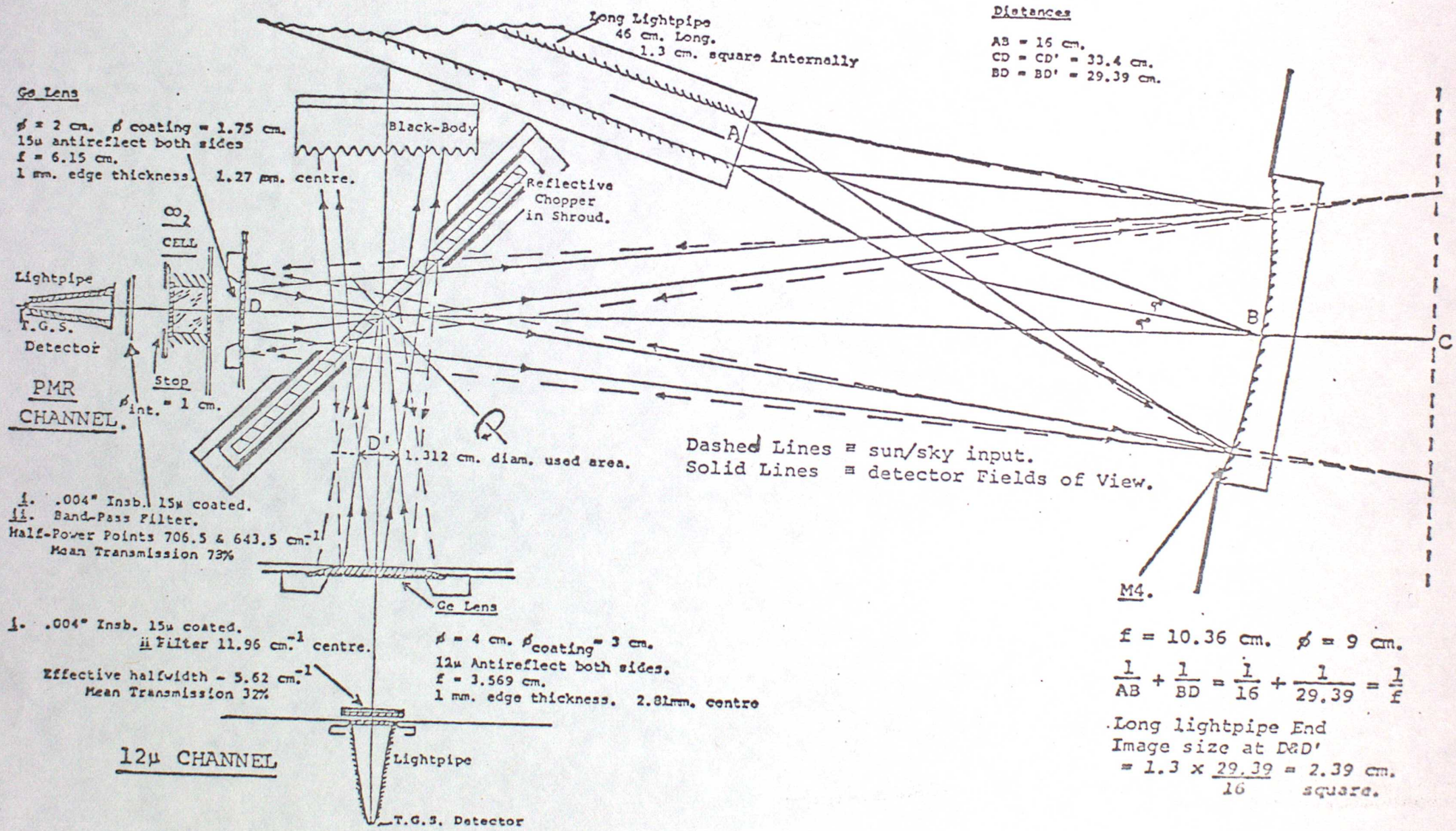

BALLOON FLIGHT SYSTEM BLOCK DIAGRAM.

FIGURE 3

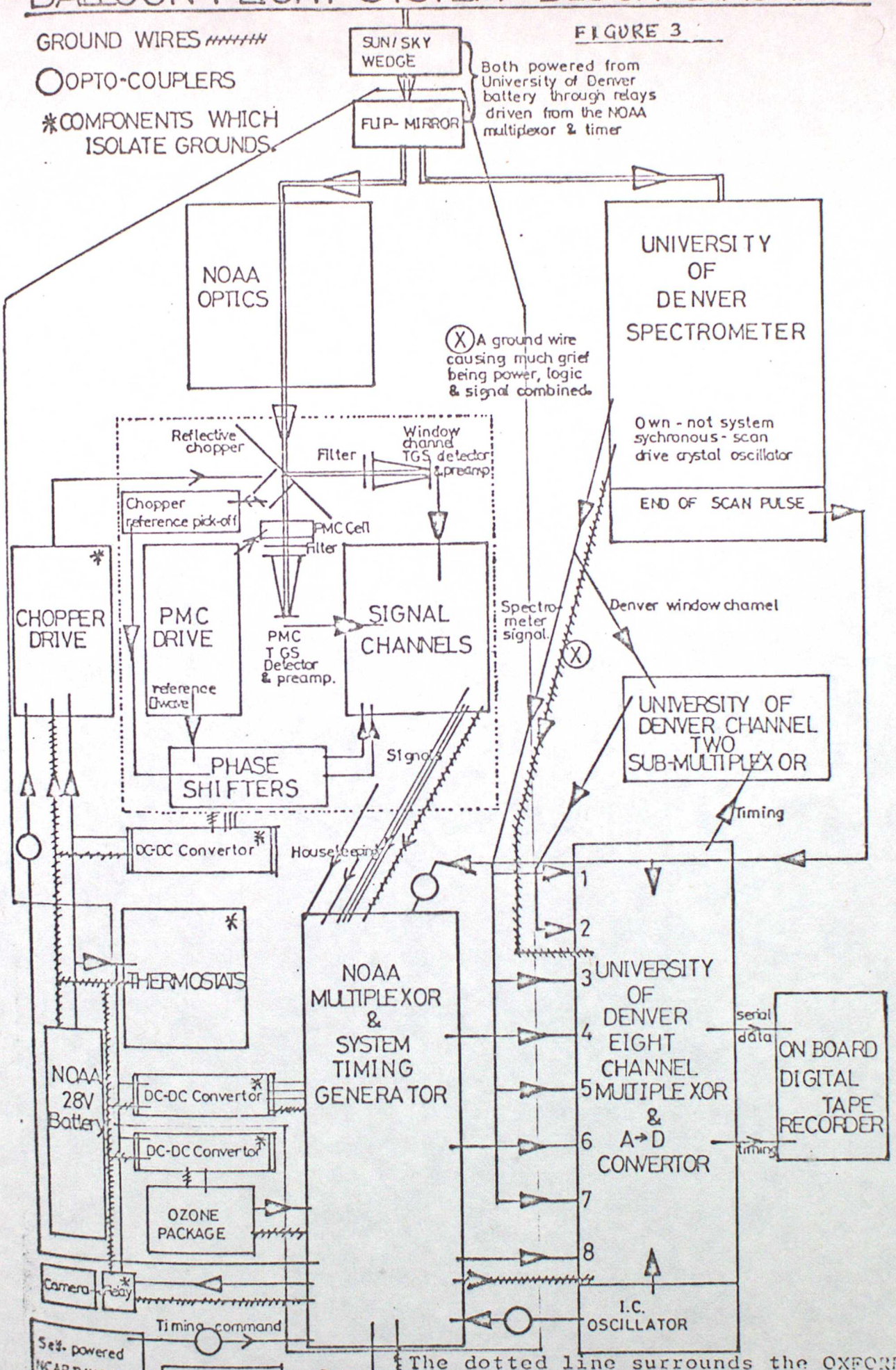

The dotted line surrounds the OXFORD sub-system, which has just one ground connection to the NOAA multiplexor. Except for one joint on the output connector, the PMR's electronics were all isolated from chassis (the box) which was itself isolated from the balloon gondola frame.

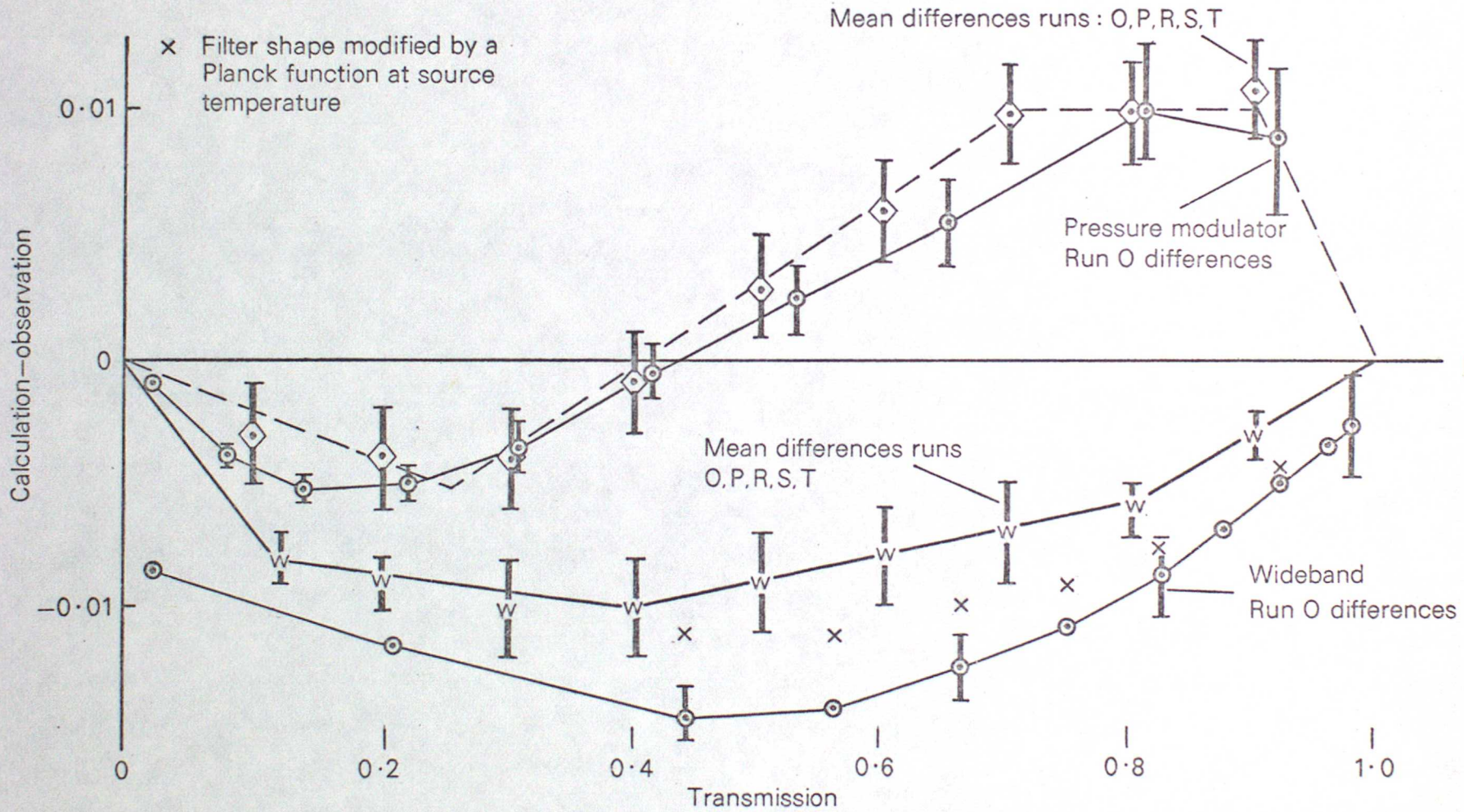

Figure 4 Run O transmission differences

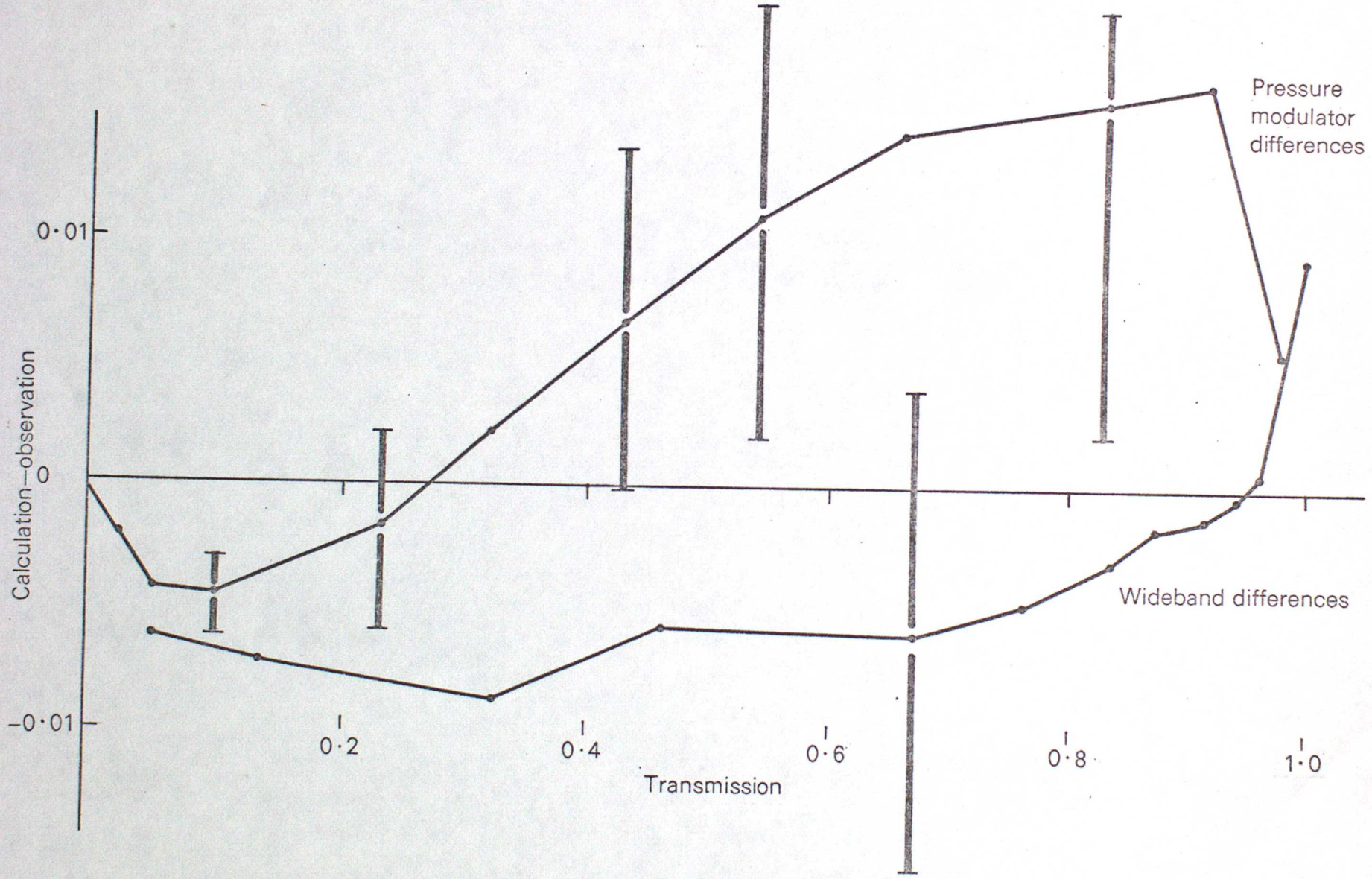

Figure 5 Run OXP transmission differences

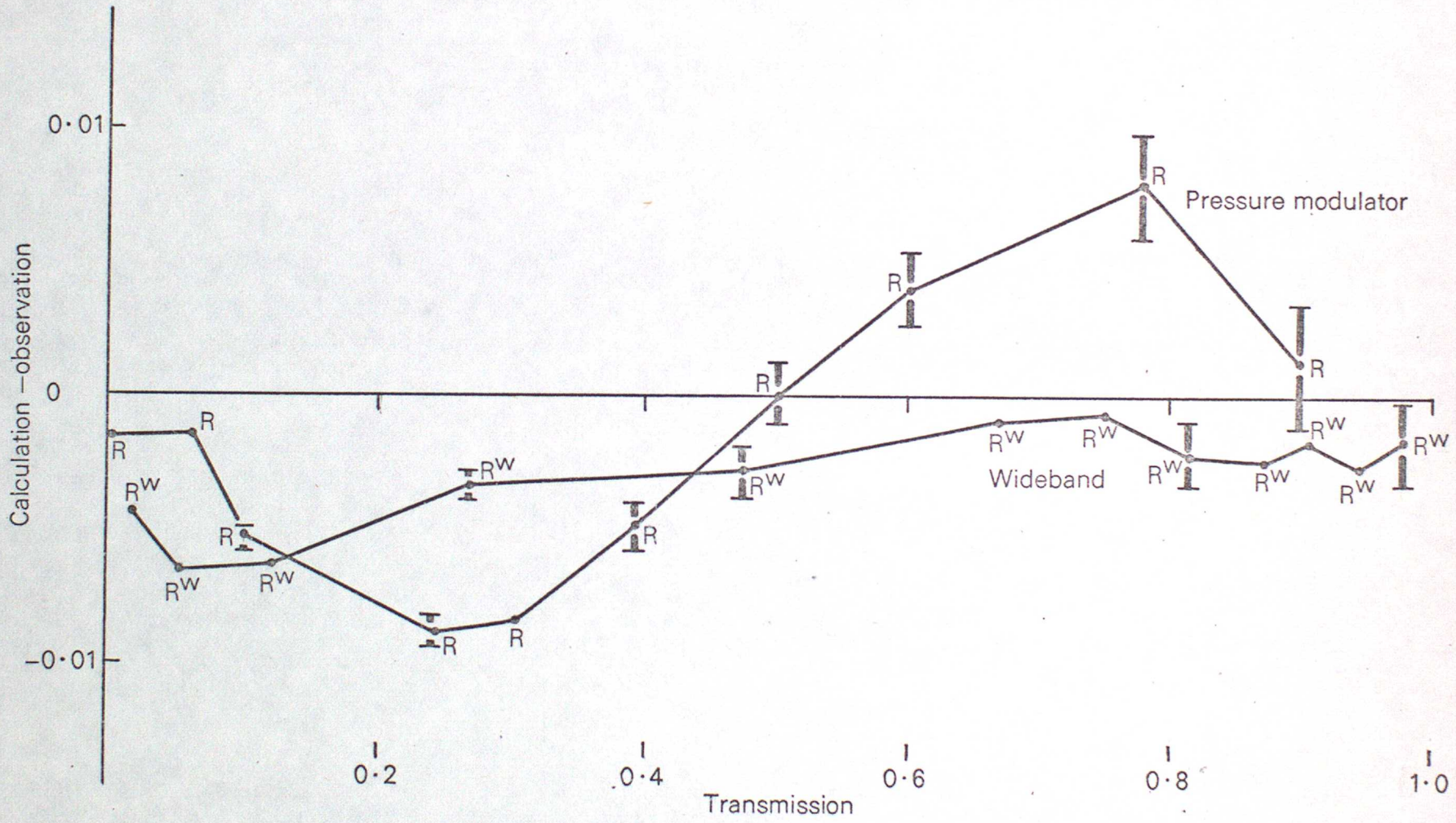

Figure 6 Run OXR transmission differences

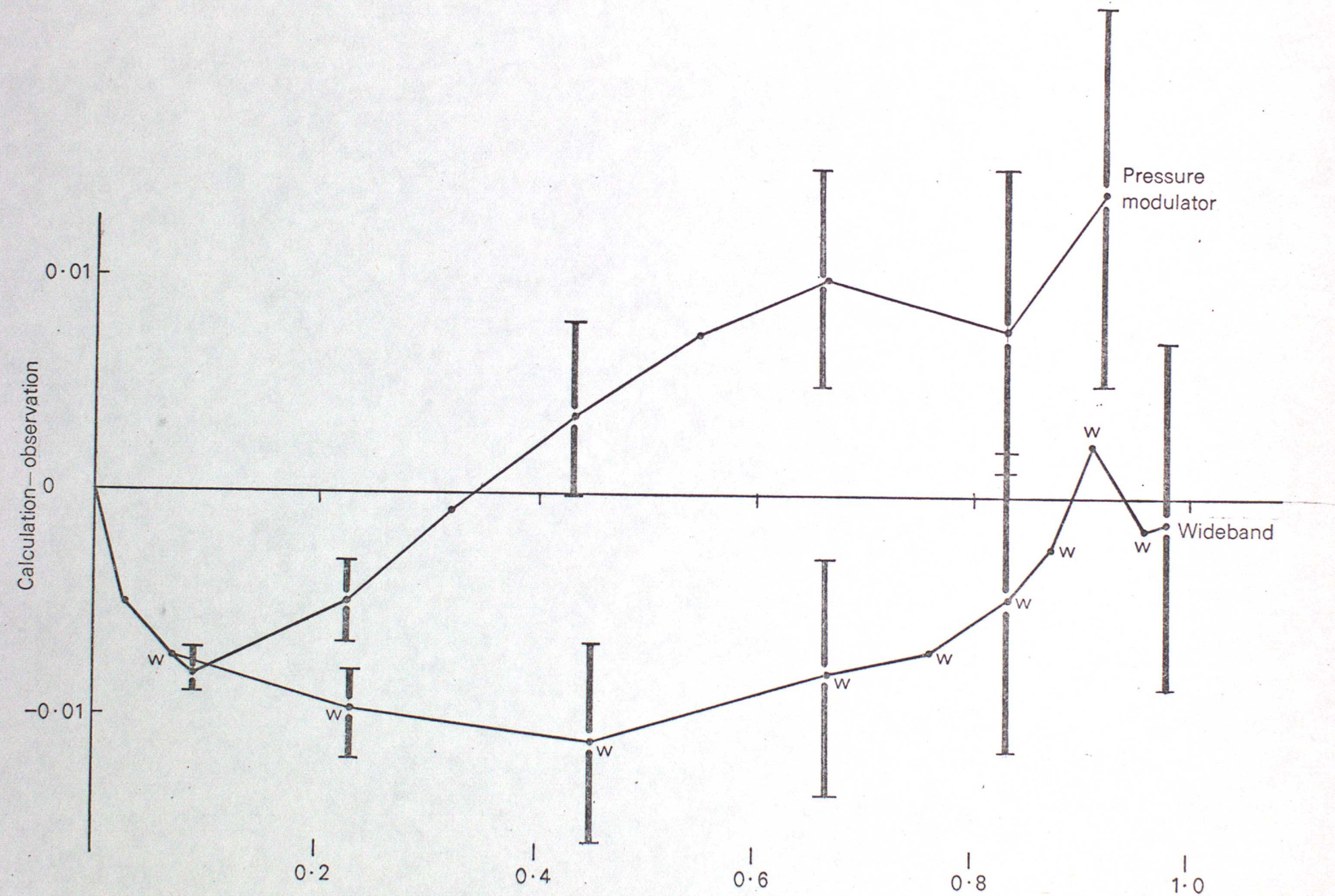

Figure 7 Run OXS Transmission differences

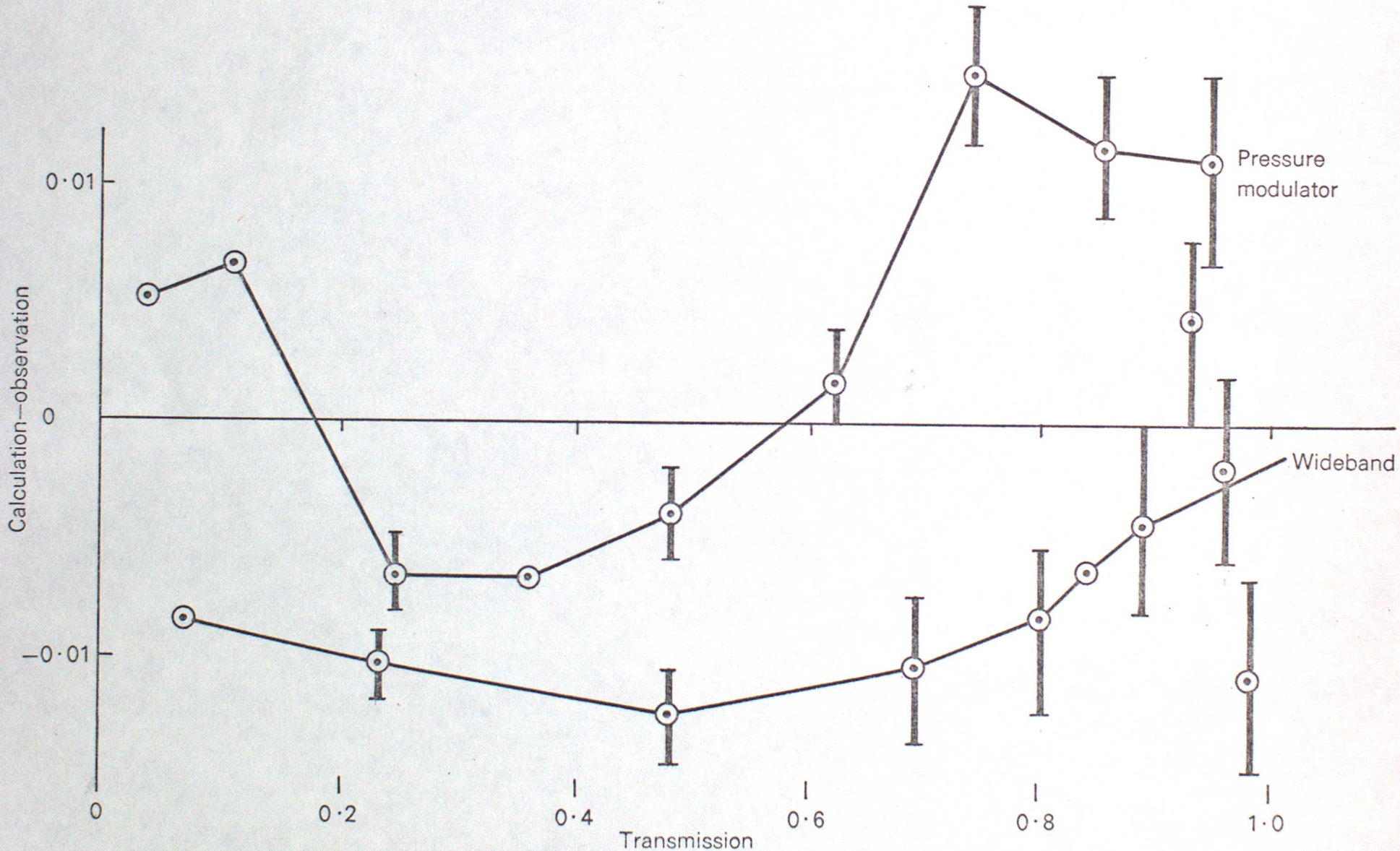

Figure 8 Run OXT Transmission differences

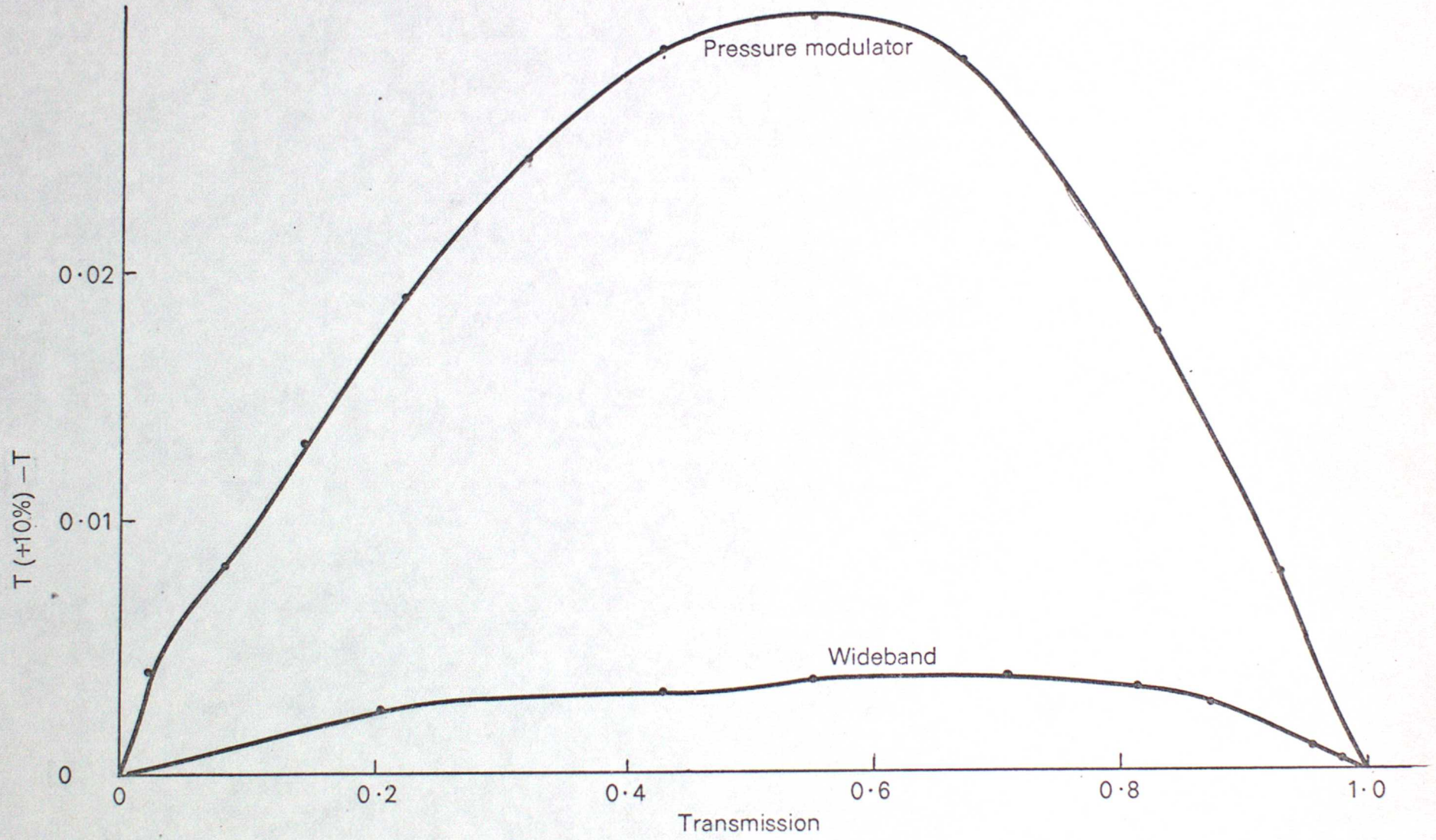

Figure 9 Plot of (calculated transmission for mean pressure 10% high−calculated transmission for mean pressure)

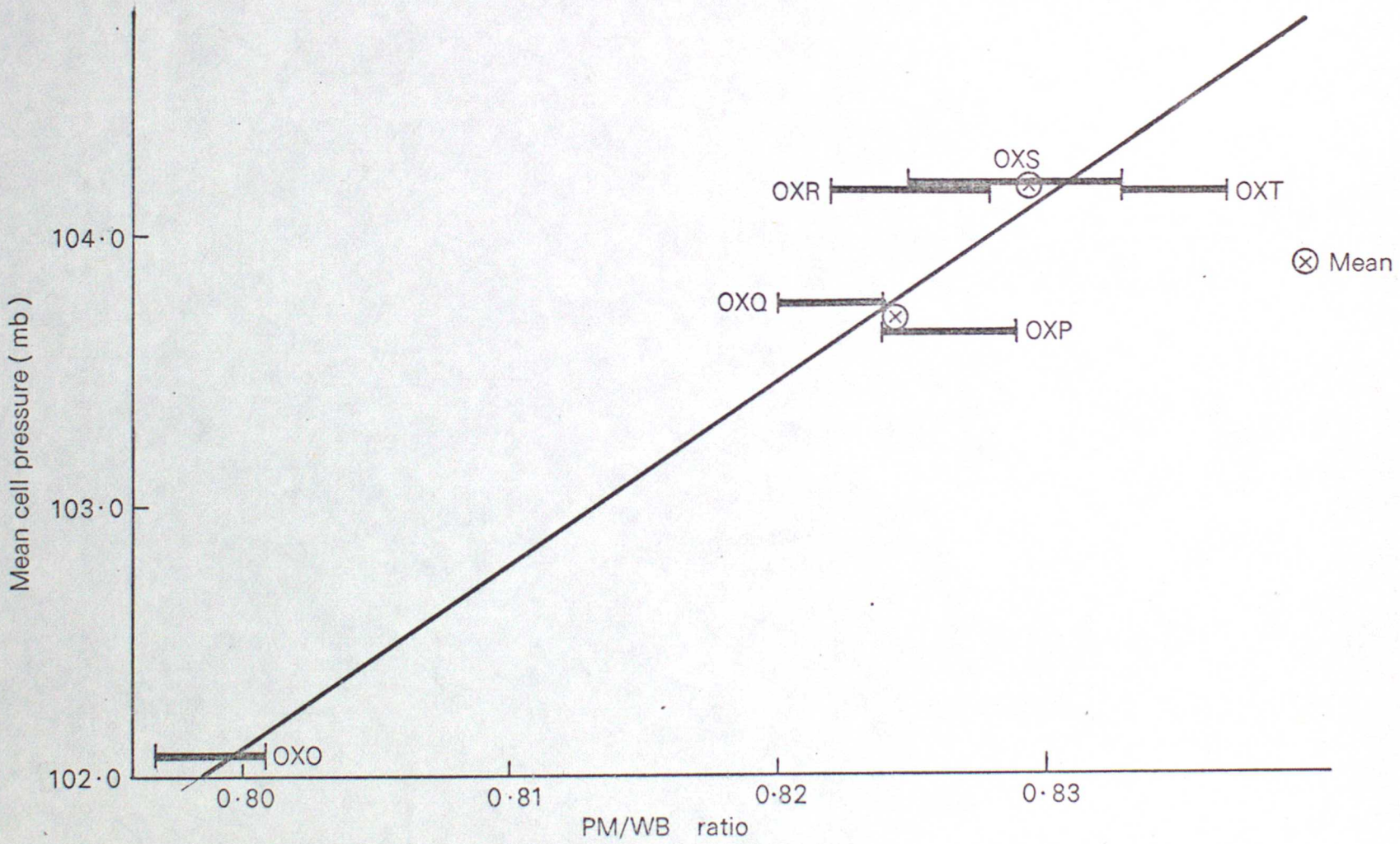

Figure 10 Plot of mean cell pressure (estimated from frequency) and the ratio of pressure modulation fullscale signal to wideband fullscale signal

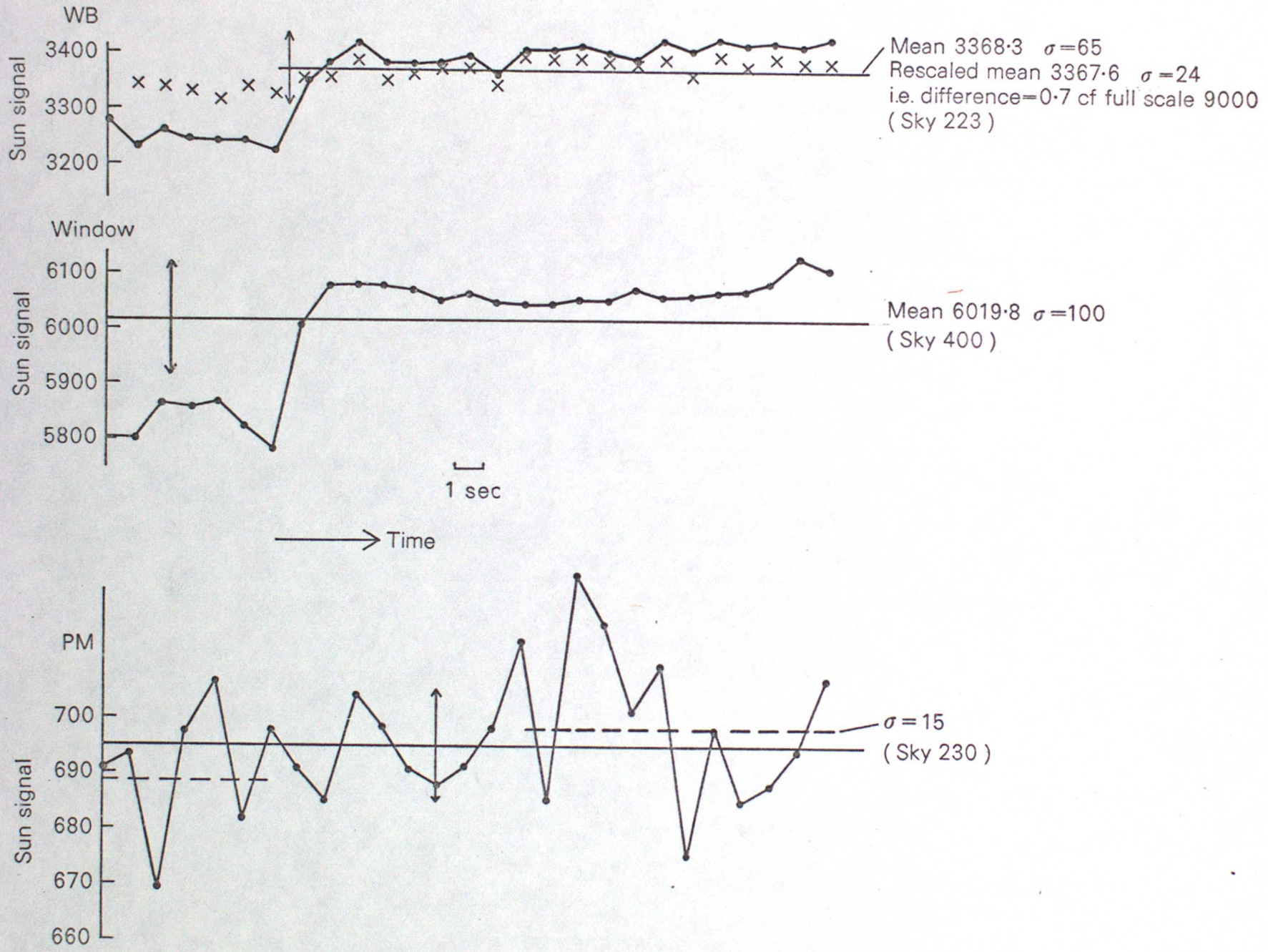

Figure 11 Demonstrating the jump in sun signal causing increase in "noise"
(at 90 mb height, block 87, Hollaman balloon flight, 17 March 1976)

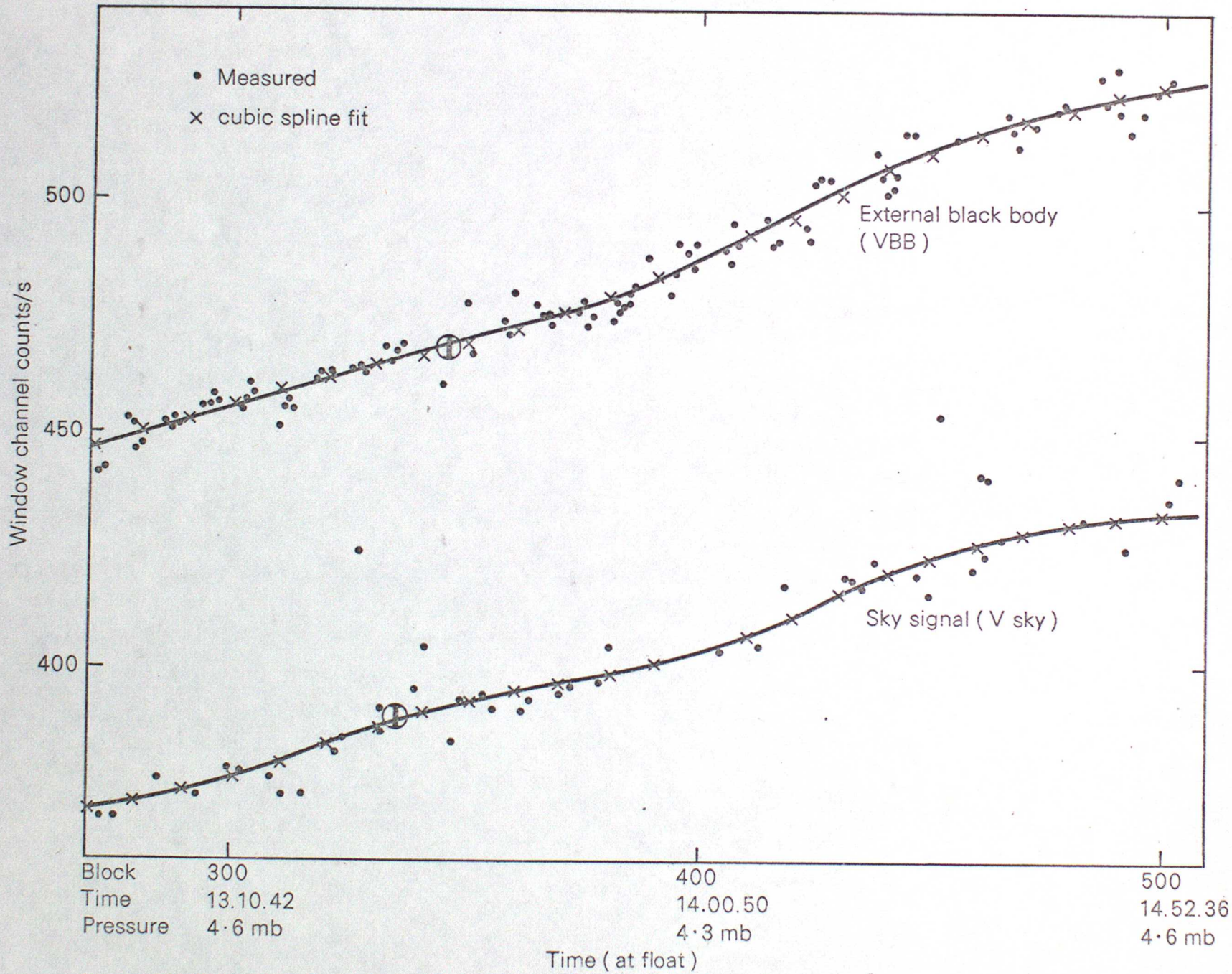

Figure 12 Illustrating the cubic spline fitting to the window sky and reference black body signals

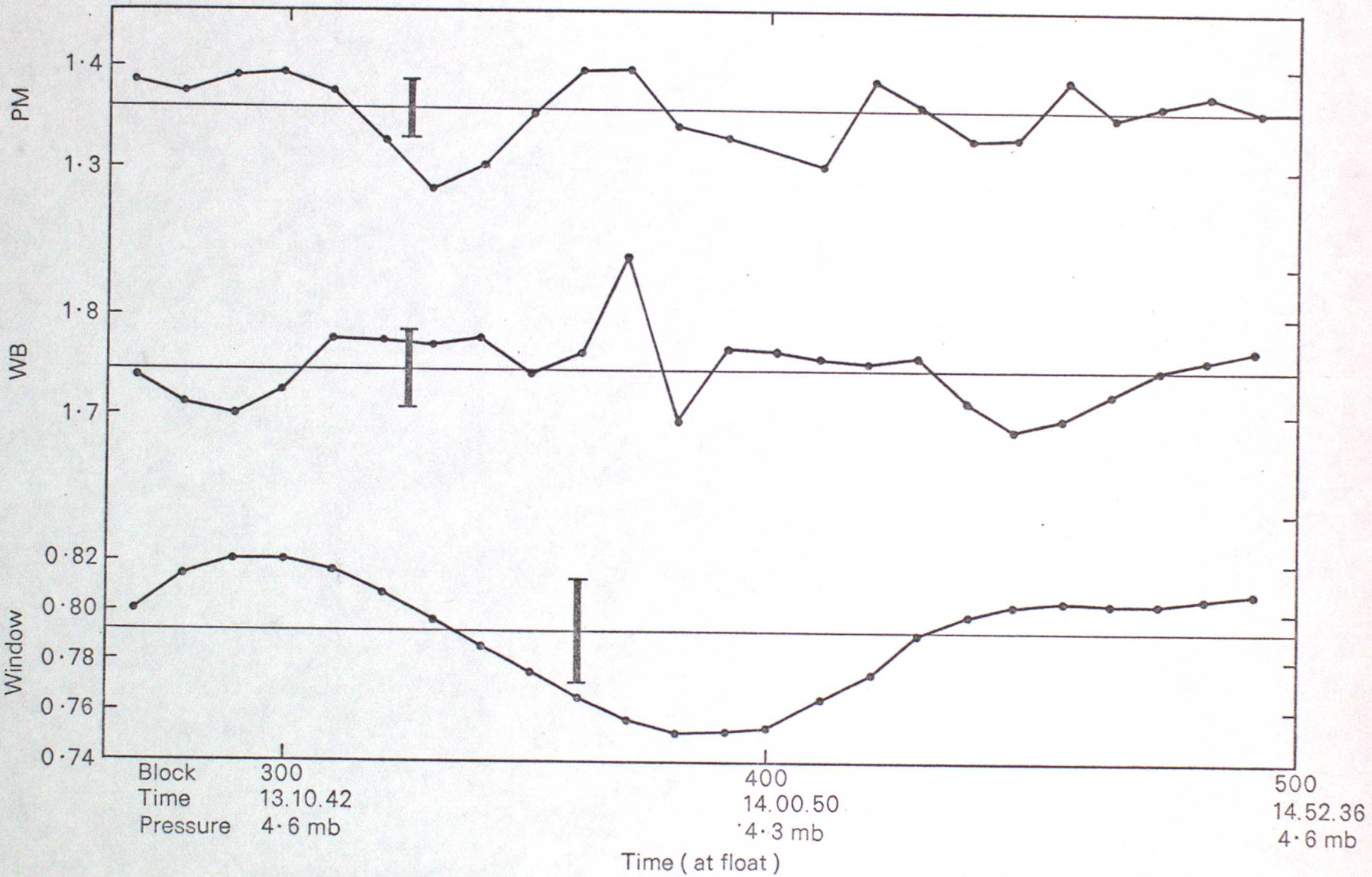

Figure 13 Plots of G response ((counts / s)/(mW / sr $cm^{-1} m^{-2}$)) for pressure modulator wideband and window channel

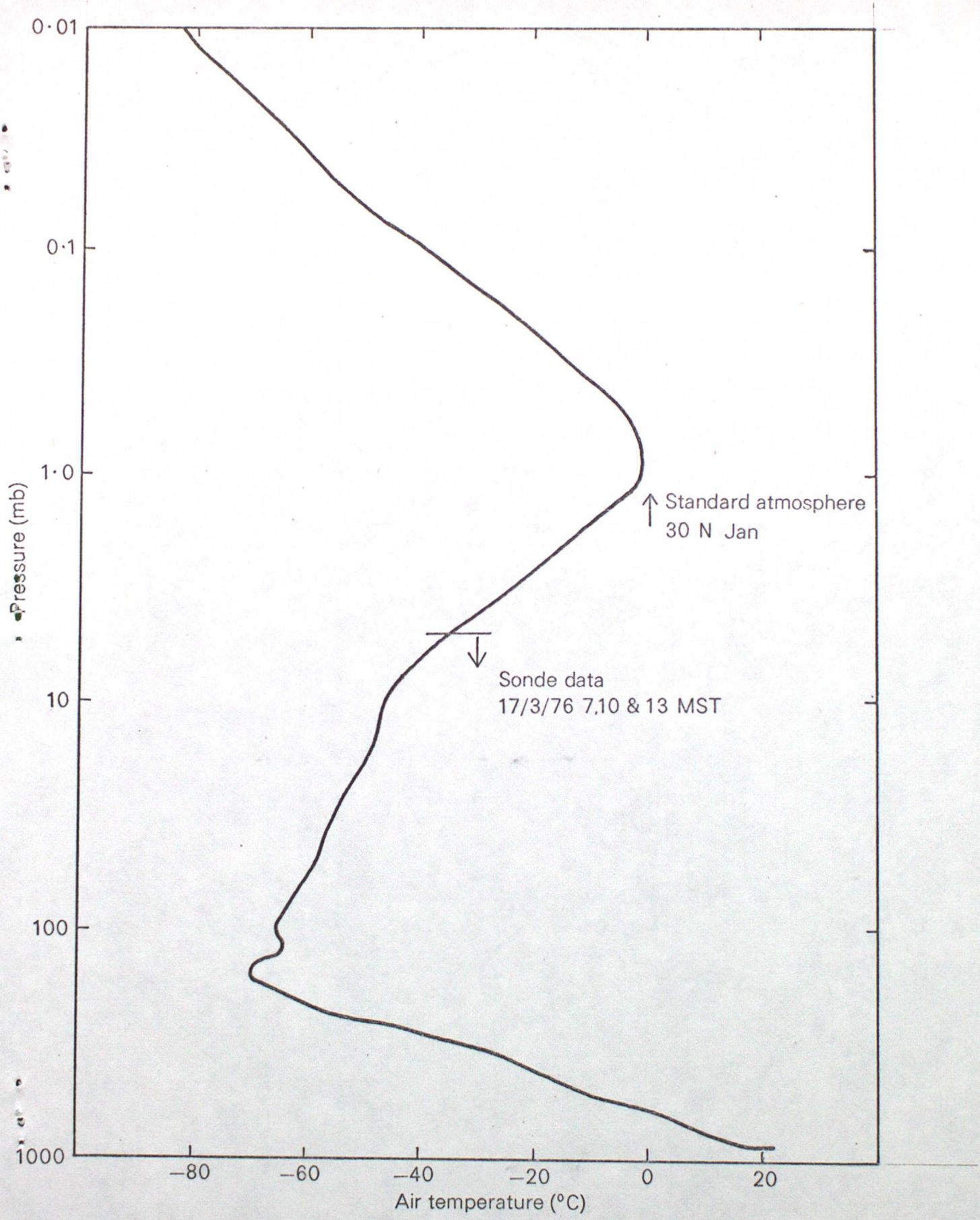

Figure 14 Atmospheric temperature profile 17 March 1976 (Hollaman)

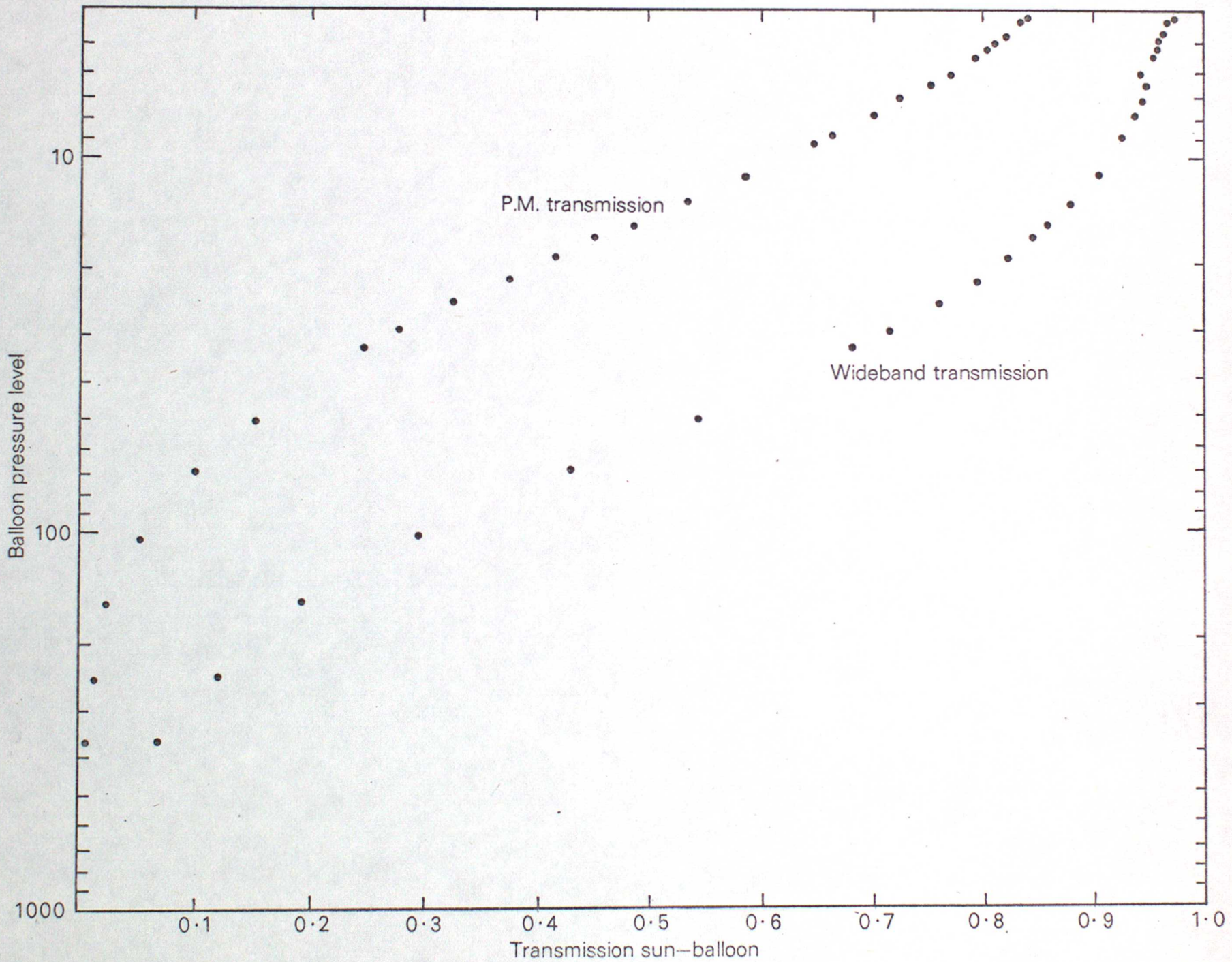

Figure 15 Transmission profile for balloon flight 17/3/78 (Hollaman)

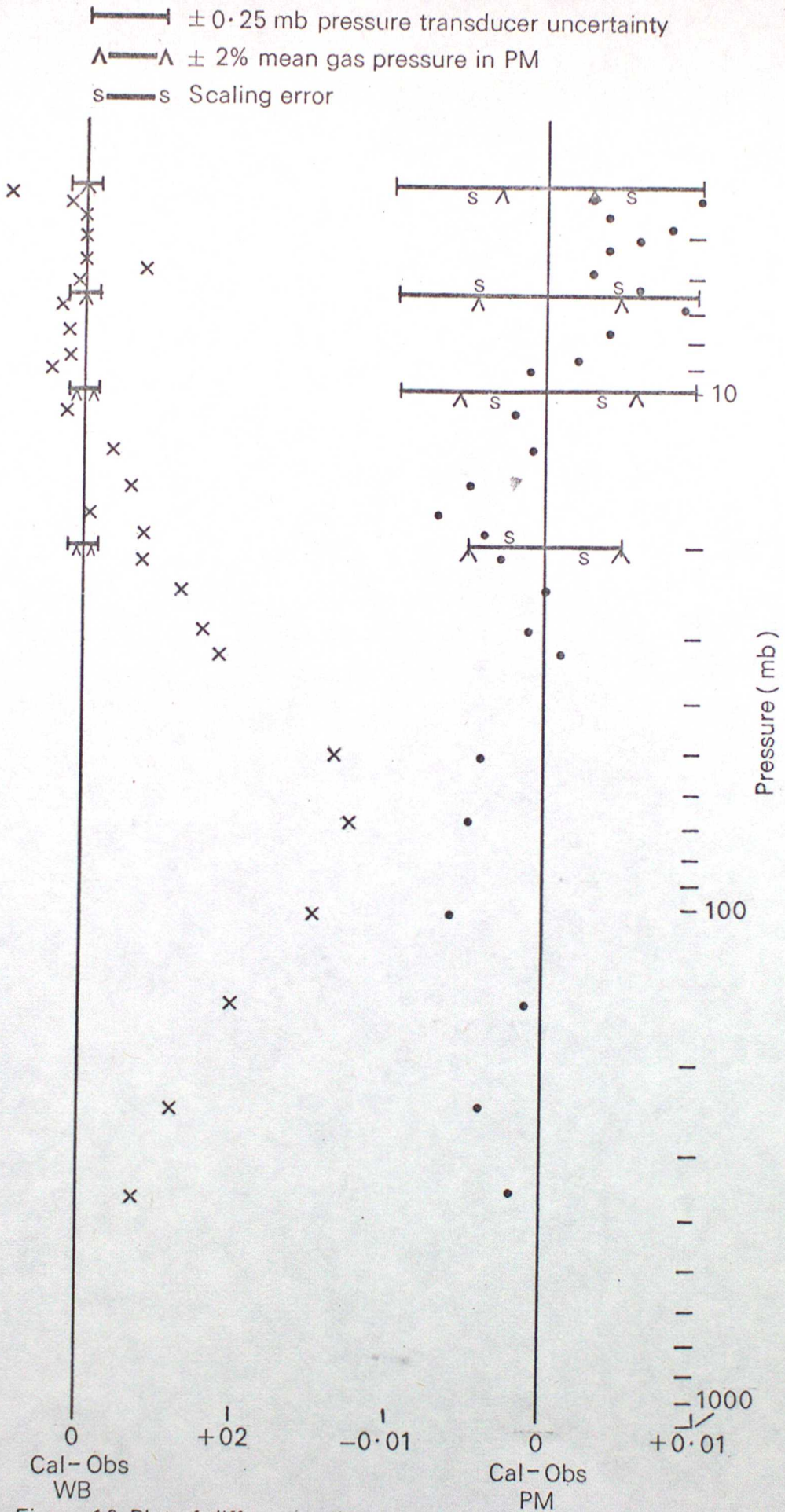

Figure 16 Plot of differences between theoretical calculations and observation